Dynamic Disorder and Fluxionality in $M_3(CO)_{12}$ Clusters: Variable-Temperature X-ray Diffraction Studies on $Fe_nRu_{3-n}(CO)_{12}$ (n = 1, 2) and the Low-Temperature Phase of $Fe_3(CO)_{12}$

Louis J. Farrugia* and Amy L. Gillon†

Department of Chemistry, University of Glasgow, Glasgow G12 8QQ, U.K.

Dario Braga

Dipartimento di Chimica "G. Ciamician", Università di Bologna, Via Selmi 2, 40126 Bologna, Italy

Fabrizia Grepioni

Dipartimento di Chimica, Via Vienna 2, Università di Sassari, 07100 Sassari, Italy

Received April 23, 1999

The metal atom disorder in the crystalline clusters $Fe_2Ru(CO)_{12}$ (**1**) and $FeRu_2(CO)_{12}$ (**2**) has been shown to be dynamic in origin. At and below 313 K, **1** crystallizes in the noncentrosymmetric space group *Pn* with two independent molecules in the asymmetric unit, both molecules having approximate C_{2v} symmetry with small C_2 distortions. Above 313 K, crystals of **1** undergo a phase transition to the centrosymmetric space group $P2_1/n$, becoming isomorphous and isostructural with the room-temperature phase of $Fe_3(CO)_{12}$ (**3**). These reversible changes are accompanied by an increase in the metal atom disorder, from a completely ordered structure at 223 K to a statistically disordered (1:1) "Star of David" structure at 323 K. Crystals of **2** show similar behavior, belonging to the noncentrosymmetric space group *C*2*cb* below 228 K and undergoing a phase transition to the centrosymmetric space group *Ccmb* above this temperature. An increase in the extent of disorder is observed in **2**, from an ordered structure at 173 K to the extended Star of David disorder above the phase transition temperature. Compound **2** has an all-terminal carbonyl arrangement, with a strong D_3 distortion, and provides the first example of the D_3 structural type for a homoleptic $M_3(CO)_{12}$ cluster. In contradiction to our earlier studies, $Fe_3(CO)_{12}$ (**3**) has now been shown to undergo a phase transition at ∼210 K to a second monoclinic phase with a partial ordering of the metal atom triangles. The asymmetric unit comprises four complete and one half-molecule of **3**, and one of these molecules (**3a**) is completely ordered. The thermal motion in **1** and the structures of **1**−**3** have been examined in the context of the various proposed fluxional mechanisms in $M_3(CO)_{12}$ clusters.

Introduction

Dynamic processes in solid organometallic complexes in general,[1] and clusters in particular,[2−4] have been studied both by X-ray crystallographic methods and by solid-state NMR. The evidence from the crystallographic studies comes from investigations into *dynamic* disorder, i.e. temperature-dependent disorder, as well as analysis of the anisotropic displacement parameters (adp's). The latter parameters are often poorly determined for metal carbonyl clusters, particularly if any disorder is present. Some of the simplest metal carbonyls show evidence for metal atom disorder, e.g. $Fe_3(CO)_{12}$,[2a−c] $Co_4(CO)_{12}$,[3a−f] $Ru_3(CO)_{12}$,[5] and $Ir_4(CO)_{12}$,[6] and there are also several examples of substituted clusters showing the same phenomenon.[2n,7] Recently it has been demonstrated that the metal atom disorder in $Co_4(CO)_{12}$,[3a] $Ru_3(CO)_{11}(L)$ (L = CN^tBu[7f,8a] and L = PMe_3),[8a] $Ru_3(CO)_9(L)_3$ (L = $P(OMe)_3$[8a] and L = PMe_3),[8b] and $Fe_2Os(CO)_{12}$[9] is dynamic in origin. While these

† Current address: School of Chemistry, University of Bristol, Bristol BS8 1TS, U.K.

(1) Braga, D. *Chem. Rev.* **1992**, *92*, 633 and references therein.

(2) (a) Wei, C. H.; Dahl, L. F. *J. Am. Chem. Soc.* **1969**, *91*, 1351 and references therein. (b) Cotton, F. A.; Troup, J. M. *J. Am. Chem. Soc.* **1974**, *96*, 4155. (c) Braga, D.; Grepioni, F.; Farrugia, L. J.; Johnson, B. F. G. *J. Chem. Soc., Dalton Trans.* **1994**, 2911. (d) Hanson, B. E.; Lisic, E. C.; Petty, J. T.; Iannoconne, G. A. *Inorg. Chem.* **1986**, *25*, 4062, (e) Dorn, H.; Hanson, B. E.; Motel, E. *Inorg. Chim. Acta* **1981**, *54*, L71. (f) Walter, T. H.; Reven, L.; Oldfield, E. *J. Phys. Chem.* **1989**, *93*, 1320. (g) Aime, S.; Gobetto, R. *J. Cluster Sci.* **1993**, *4*, 1. (h) Grandjean, F.; Long, G. L.; Benson, C. G.; Russo, U. *Inorg. Chem.* **1988**, *27*, 1524. (i) Grandjean, F.; Long, G. L. *Inorg. Chem.* **1996**, *35*, 4532. (j) Braga, D.; Anson, C. E.; Bott, A.; Johnson, B. F. G.; Marseglia, E. *J. Chem. Soc., Dalton Trans.* **1990**, 3517. (k) Johnson, B. F. G.; Bott, A. *J. Chem. Soc., Dalton Trans.* **1990**, 2437. (l) Johnson, B. F. G.; Roberts, Y. V.; Parisini, E. *J. Chem. Soc., Dalton Trans.* **1992**, 2573. (m) Johnson, B. F. G.; Roberts, Y. V. *J. Chem. Soc., Dalton Trans.* **1993**, 2945. (n) Adams, H.; Bailey, N. A.; Bentley, G. W.; Mann, B. E. *J. Chem. Soc., Dalton Trans.* **1989**, 1831. (o) Hawkes, G. E.; Sales, K. D.; Lian, L. Y.; Gobetto, R. *Proc. R. Soc. London, A* **1989**, *424*, 93. (p) Corradini, P.; Paiaro, G. *Ric. Sci.* **1966**, *36*, 365. (q) Lentz, D.; Marschall, R. *Organometallics* **1991**, *10*, 1487.

10.1021/om9902986 CCC: $18.00
Publication on Web 11/22/1999

studies have clear implications for the mechanisms of fluxionality, it is often difficult to draw unambiguous conclusions from the X-ray data alone. Thus, in the case of $Fe_2Os(CO)_{12}$ we have shown that the dynamic metal atom disorder requires an *effective* rotation of the metal triangle by 180° about the pseudo 3-fold axis, while the solid-state NMR data indicates this most likely occurs via intermediate 60° rotations.[9]

The archetypal carbonyl cluster showing metal atom disorder is $Fe_3(CO)_{12}$.[2a−c] Wei and Dahl[2a] first demonstrated the statistical "Star of David" disorder in the metal triangle, and the structure was then further refined by Cotton and Troup.[2b] There is an ongoing controversy in the literature regarding the exact mechanism of solution and solid-state fluxionality of this highly dynamic molecule. Johnson[2j−m,3h,10] has proposed that the lowest energy process in both phases is a C_2 libration of the Fe_3 triangle relative to the ligand polyhedron (which is approximately, but not exactly, an icosahedron[2a,p]). In essence, it is proposed that the Fe_3 triangle librates about the molecular C_2 axis by ∼18° to give a D_3 structure, which can then revert to the ground-state C_{2v}/C_2 structure by re-formation of the carbonyl bridges along either of the three (now equivalent) Fe−Fe edges. Mann[11] has offered an alternative mechanism, the "concerted bridge-opening bridge-closing" mechanism[2n] (or S_{10} rotation mechanism), whereby the Fe_3 triangle (or ligand polytope) is rotated about one of the pseudo-S_{10} axes which is parallel to the Fe−Fe bond linking the unique Fe atom to one of the pair of equivalent Fe atoms. This mechanism also results in the movement of the carbonyl-bridged Fe−Fe edge around the Fe_3 triangle. An animation of Mann's proposed mechanism may be viewed on the World Wide Web.[12] Both of these mechanisms retain the antipodal relationships of the ligand polyhedron. Other proposals for fluxionality in $Fe_3(CO)_{12}$ and its derivative in the solid state and solution include the Cotton and Troup[2b] "merry-go-round" mechanism involving a localized bridge-terminal exchange, the C_3 jump mechanism of Hanson *et al.*,[2d] and the alternative S_{10} rotation mechanism of Lentz and Marschall.[2q] The reader is referred to recent Dalton Perspectives[11,13,14] and our earlier work[2c] for further details on these proposed fluxional mechanisms in $Fe_3(CO)_{12}$ and its derivatives.

In this article we describe the variable-temperature X-ray structures of the closely related clusters $Fe_2Ru(CO)_{12}$ (**1**) and $FeRu_2(CO)_{12}$ (**2**) and the low-temperature phase of $Fe_3(CO)_{12}$ (**3**) and consider the implications for fluxionality in these molecules. Preliminary aspects of some of this work have been previously reported.[14,15]

Experimental Section

Samples of $Fe_2Ru(CO)_{12}$,[16] $FeRu_2(CO)_{12}$[17] and $Fe_3(CO)_{12}$[18] were prepared by literature methods, and recrystallized from dichloromethane/hexane solutions to give crystals suitable for the single-crystal studies.

Studies on $Fe_2Ru(CO)_{12}$ (1) and $FeRu_2(CO)_{12}$ (2). Crystals of suitable size were attached to glass fibers using acrylic resin and mounted on a goniometer head in a general position. Data were collected in the bisecting mode using graphite-monochromated X-radiation ($\lambda = 0.710\ 73$ Å) on either Enraf-Nonius CAD4 (Glasgow and Bologna) or Siemens P4 (Glasgow) diffractometers equipped with serial detectors and low-temperature devices. For **1**, data were collected at 223 K (Glasgow), 298 K (Glasgow), 313 K (Bologna) and 323 K (Bologna). For **2** data were collected in Glasgow (Siemens P4 unless otherwise indicated) at 173, 223, 228, 233, 243, and 291 K (CAD4). The phase transition temperature of 230(±5) K for **2** was established from axial photographs taken at 3 K temperature intervals in the range 223−238 K. The data sets at 228 and 233 K were too close to the phase-transition temperature to be considered reliable, in view of the temperature instability (±5 K) of the Siemens P4. Details of data collection procedures and structure refinements for representative studies at the low- and high-temperature limits are given in Table 1. Precise unit cell dimensions were determined by refinement of the setting angles of high-angle reflections. Standard reflections were measured every 2 h during data collection, and an interpolated correction was applied to the reflection data where necessary. Lorentz−polarization corrections were then applied to the reflection data. Data were corrected for absorption either by semiempirical ψ-scans[19] or by the method of Stuart and

(3) (a) Farrugia, L. J.; Braga, D.; Grepioni, F. *J. Organomet. Chem.* **1999**, *573*, 60. (b) Corradini, P. *J. Chem. Phys.* **1959**, *31*, 1676. (c) Corradini, P.; Sirugu, A. *Ric. Sci.* **1966**, *36*, 188. (d) Wei, C. H.; Dahl, L. F. *J. Am. Chem. Soc.* **1966**, *88*, 1821. (e) Wei, C. H. *Inorg. Chem.* **1969**, *8*, 2384. (f) Carré, F. H.; Cotton, F. A.; Frenz, B. A. *Inorg. Chem.* **1976**, *15*, 380. (g) Hanson, B. E.; Lisic, E. C. *Inorg. Chem.* **1986**, *25*, 716. (h) Anson, C. E.; Benfield, R. E.; Bott, A. W.; Johnson, B. F. G.; Braga, D.; Marseglia, E. *J. Chem. Soc., Chem. Commun.* **1988**, 889. (i) Aime, S.; Botta, M.; Gobetto, R.; Hanson, B. E. *Inorg. Chem.* **1989**, *28*, 1196. (j) Heaton, B. T.; Sabounchei, J.; Kernaghan, S.; Nakayama, H.; Eguchi, T.; Takeda, S.; Nakamura, N.; Chihara, H. *Bull. Chem. Soc. Jpn.* **1990**, *63*, 3019. (k) Eguchi, T.; Nakayama, H.; Ohki, H.; Takeda, S.; Nakamura, N.; Kernaghan, S.; Heaton, B. T. *J. Organomet. Chem.* **1992**, *428*, 207.

(4) (a) Braga, D.; Heaton, B. T. *J. Chem. Soc., Chem. Commun.* **1987**, 608. (b) Eguchi, T.; Harding, R. A.; Heaton, B. T.; Longoni, G.; Miyagi, K.; Näring, J.; Kakamura, N.; Nakayama, H.; Smith, A. K. *J. Chem. Soc., Dalton Trans.* **1997**, 479. (c) Eguchi, T.; Heaton, B.; Harding, R.; Miyagi, K.; Longoni, G.; Näring, J.; Kakamura, N.; Nakayama, H.; Pakkanen, T. A.; Pursiainen, J.; Smith, A. K. *J. Chem. Soc., Dalton Trans.* **1996**, 625. (d) Harding, R. A.; Nakayama, H.; Eguchi, T.; Nakamura, N.; Heaton, B. T.; Smith, A. K. *Polyhedron* **1998**, *17*, 2857. (e) Barkley, J. V.; Eguchi, T.; Harding, R. A.; Heaton, B. T.; Longoni, G.; Manzi, L.; Nakayama, H.; Miyagi, K.; Smith, A. K.; Steiner, A. *J. Organomet. Chem.* **1999**, *573*, 254. (f) Aime, S.; Gobetto, R.; Orlandi, A.; Groombridge, C. J.; Hawkes, G. E.; Mantle, M. D.; Sales, K. D. *Organometallics* **1994**, *13*, 2375.

(5) Pursiainen, J.; Pakkanen, T. A.; Ahlgrén, M.; Valkonen, J. *Acta Crystallogr., Sect. C* **1993**, *C49*, 1142

(6) Churchill, M. R.; Hutchison, J. P. *Inorg. Chem.* **1978**, *17*, 3528.

(7) (a) Alex, R. F.; Einstein, F. W. B.; Jones, R. H.; Pomeroy, R. K. *Inorg. Chem.* **1987**, *26*, 3175. (b) Bruce, M. I.; Liddell, M. J.; Hughes, C. A.; Skelton, B. W.; White, A. H. *J. Organomet. Chem.* **1988**, *347*, 157. (c) Bruce, M. I.; Liddell, M. J.; Hughes, C. A.; Patrick, J. M.; Skelton, B. W.; White, A. H. *J. Organomet. Chem.* **1988**, *347*, 181. (d) Bruce, M. I.; Liddell, M. J.; Hughes, C. A.; Bytheway, I.; Skelton, B. W.; White, A. H. *J. Organomet. Chem.* **1988**, *347*, 217. (e) Bruce, M. I.; Matisons, J. G.; Skelton, B. W.; White, A. H. *J. Chem. Soc., Dalton Trans.* **1983**, 2375. (f) Bruce, M. I.; Pain, G. N.; Hughes, C. A.; Patrick, J. M.; Skelton, B. W.; White, A. H. *J. Organomet. Chem.* **1986**, *307*, 343. (g) Bruce, M. I.; Skelton, B. W.; White, A. H.; Zaitseva, N. N. *Aust. J. Chem.* **1997**, *50*, 163. (h) $Fe_3(CO)_{11}\{P(OMe)_3\}$: Adams, H.; Chen, X.; Heath, S.; Mann, B. E. Unpublished work. See also ref 12.

(8) (a) Farrugia, L. J.; Rosenhahn, C.; Whitworth, S. *J. Cluster Sci.* **1998**, *9*, 505. (b) Farrugia, L. J.; Paterson, C. Unpublished results.

(9) Farrugia, L. J.; Senior, A. M.; Braga, D.; Grepioni, F.; Orpen, A. G.; Crossley, J. G. *J. Chem. Soc., Dalton Trans.* **1996**, 631.

(10) (a) Johnson, B. F. G.; Roberts, Y. V. *Polyhedron* **1993**, *12*, 977. (b) Johnson, B. F. G.; Roberts, Y. V. *J. Chem. Soc., Dalton Trans.* **1993**, 2945. (c) Johnson, B. F. G.; Benfield, R. E. *J. Chem. Soc., Dalton Trans.* **1978**, 1554.

(11) Mann, B. E. *J. Chem. Soc., Dalton Trans.* **1997**, 1457.

(12) http://www.rsc.org/is/journals/current/dalton/fe3carb.htm.

(13) Johnson, B. F. G. *J. Chem. Soc., Dalton Trans.* **1997**, 1473.

(14) Farrugia, L. J. *J. Chem. Soc., Dalton Trans.* **1997**, 1783.

(15) Braga, D.; Farrugia, L. J.; Gillon, A. L.; Grepioni, F.; Tedesco, E. *Organometallics* **1996**, *15*, 4684.

(16) Venäläinen, T.; Pakkanen, T. *J. Organomet. Chem.* **1986**, *316*, 183.

(17) Yawney, D. B. W.; Stone, F. G. A. *J. Chem. Soc. A* **1969**, 502.

(18) McFarlane, W.; Wilkinson, G. *Inorg. Synth.* **1966**, *8*, 181.

(19) North, A. C. T.; Phillips, D. C.; Mathews, F. S. *Acta Crystallogr., Sect. A* **1968**, *A24*, 351.

Table 1. Experimental Details of the Crystallographic Studies[a]

	1	1	2	2	3
formula	$C_{12}Fe_2O_{12}Ru$	$C_{12}Fe_2O_{12}Ru$	$C_{12}FeO_{12}Ru_2$	$C_{12}FeO_{12}Ru_2$	$C_{12}Fe_3O_{12}$
color	black	black	black	black	black
temp/K	223	323	173	291	123
M_r	548.89	548.89	594.11	594.11	503.67
space group	*Pn*	$P2_1/n$	*C2cb*	*Ccmb*	$P2_1/c$
cryst syst	monoclinic	monoclinic	orthorhombic	orthorhombic	monoclinic
a/Å	8.3068(8)	8.400(5)	11.6326(12)	11.6581(3)	19.520(3)
b/Å	22.468(3)	11.420(5)	12.8789(13)	13.1117(14)	33.408(8)
c/Å	8.8830(13)	8.943(5)	22.639(4)	11.5085(8)	11.261(2)
β/deg	96.531(9)	96.84(6)	90	90	102.950(10)
V/Å^{-3}	1647.1(4)	851.8(8)	3391.6(7)	1759.2(2)	7157(2)
θ range for cell/deg	17.5−21.6	9.5−12.3	6.3−25.0	17.6−21.4	5−25
Z	4	2	8	4	18
D_{calcd}/g cm^{-3}	2.213	2.14	2.327	2.243	2.104
F(000)	1056	528	2256	1128	4428
μ(Mo Kα)/cm^{-1}	27.07	26.18	26.65	25.69	27.66
scan mode	$\varpi/2\theta$	$\varpi/2\theta$	$\theta/2\theta$	$\varpi/2\theta$	n/a
θ range/deg	2.5−25.0	2.9−25.0	2.5−30.0	2.9−25.0	1.2−27.6
cryst size/mm	0.3 × 0.3 × 0.25	0.4 × 0.4 × 0.3	0.37 × 0.37 × 0.25	0.37 × 0.37 × 0.25	0.3 × 0.25 × 0.25
no. of data collected	3830	1550	3106	1083	44191
no. of unique data	3505	1454	2758	813	16288
abs cor	ψ scans	DIFABS	DIFABS	ψ scans	none
min/max transmissn factors	0.832−0.999	0.421−0.507	0.439−0.555	0.846−0.999	n/a
hkl range	−9 to +9; −2 to +26; −10 to +1	−9 to +9; 0−13; 0−10	−4 to +15; −4 to +18; −31 to +30	−1 to +13; −2 to +15; −1 to +13	−24 to +25; −37 to +43; −14 to +12
R_{int}	0.0102	0.035	0.039	0.013	0.089
std rflns	(1,2,−4), (1,10,−1), (4,−1,0)	(1,−2,3), (2,1,−4)	(423), (043), (372)	(−5,−1,3), (153), (−3,3,−3)	n/a
no. of data in refinement	3505	1454	2698	813	16 288
no. of refined params	489	185	246	105	1167
final R1, $I > 2\sigma(I)$ (all data)	0.024 (0.025)	0.065 (0.069)	0.037 (0.056)	0.038 (0.046)	0.060 (0.169)
wR2, $I > 2\sigma(I)$ (all data)	0.063 (0.064)	0.187 (0.194)	0.087 (0.111)	0.108 (0.114)	0.108 (0.131)
goodness of fit *S*	1.048	1.102	1.130	1.129	0.726
weighting params *A* and *B*	0.0482, 0.9483	0.1363, 0.9658	0.0296, 53.55	0.0610, 4.0835	0.0286, 0.0
Flack absolute structure param	0.46(3)	n/a	0.47(13)	n/a	n/a
largest remaining feature in electron density map/e Å^{-3}	0.65 (max), −0.51 (min)	1.07 (max), −0.71 (min)	1.22 (max), −1.53 (min)	0.77 (max), −0.50 (min)	1.68 (max), −1.93 (min)
shift/esd in last cycle (max)	0.001	0.004	0.001	0.001	0.013

[a] Definitions: $R1 = \sum(||F_o| - |F_c||)/\sum(F_o)$; $wR2 = \{\sum(w(F_o^2 - F_c^2)^2)/\sum(w(F_o^2)^2)\}^{1/2}$; $R_{int} = \sum|F_o^2 - F_o^2(\text{mean})|/\sum F_o^2$ (summation is carried out only where more than one symmetry equivalent is averaged); weight $w = [\sigma^2(F_o^2) + (AP)^2 + BP]^{-1}$, where $P = F_o^2/3 + 2F_c^2/3$.

Walker.[20] The structure of **1** was solved by direct methods (SIR-92[21]) without problems, but all attempts to solve the centrosymmetric structure of **2** at 291 K by automatic Patterson or direct methods failed. The structure was finally solved intuitively by guessing that the metal triangle was situated at an inversion center as in $Fe_3(CO)_{12}$ and translating an incorrect solution obtained by direct methods. All atoms were allowed anisotropic thermal motion, except for the low-occupancy disordered metal positions and the C atoms in **1** at 323 K. Refinement (SHELXL-97[22]) was by full-matrix least squares on F^2, using all the unique data and the weighting scheme $w = [\sigma^2(F_o)^2 + (AP)^2 + BP]^{-1}$, where $P = F_o^2/3 + 2F_c^2/3$. The values of the Flack parameters for the noncentrosymmetric phases of **1** and **2** (~0.45; see Table 1) indicates that both are racemic twins. All calculations were carried out using the WinGX package,[23] and thermal ellipsoid plots were obtained using the program ORTEP-3 for Windows.[24]

Studies on $Fe_3(CO)_{12}$ (3). Diffraction data on $Fe_3(CO)_{12}$ were collected on a Siemens SMART three-circle diffractometer equipped with a CCD area detector, either using a laboratory source of graphite-monochromated Mo Kα X-radiation (λ = 0.710 73 Å) or synchrotron radiation (λ = 0.6870 Å) at station 9.8 of the SRS, CLRC, Daresbury, U.K. Crystals were initially examined at room temperature. Unit cells were obtained from 3 sets of 30 matrix frames which were oriented such that orthogonal wedges of reciprocal space were surveyed. Full sets of intensities were integrated from series of ω-rotation exposures with different ϕ angles, chosen to generate more than a hemisphere of data. Each exposure covered 0.3° in ω.

Examination of the room-temperature matrix frames clearly showed areas of diffuse but structured scattering at low θ angles, which is indicative of significant disorder. When the temperature was below 210 K, this diffuse scattering was substantially reduced, but many more diffraction maxima were observed, indicating a phase transition to a larger unit cell. The new phase below ~210 K (the LT phase) has a unit cell

(20) Walker, N.; Stuart, D. *Acta Crystallogr., Sect. A* **1983**, *A39*, 158.
(21) SIR-92: Altomare, A.; Cascarano, G.; Giacovazzo, C.; Guagliardi, A. *J. Appl. Crystallogr.* **1993**, *26*, 343.
(22) Sheldrick, G. M. SHELXL-97 (release 97-2); Institüt für Anorganische Chemie der Universität, Tammanstrasse 4, D-3400 Göttingen, Germany, 1998.
(23) Farrugia, L. J. *J. Appl. Crystallogr.* **1999**, *32*, 837.
(24) Farrugia, L. J. *J. Appl. Crystallogr.* **1997**, *30*, 565.

which is a supercell of the room-temperature (RT) phase, with 9 times the volume. This supercell is clearly related to the RT unit cell: the LT *a* axis is the RT [−2,0,1] lattice vector and the LT *c* axis is the RT [101] lattice vector, while the LT *b* axis is the tripled RT *b* axis [030]. Moreover, it is possible to index a subset (one-ninth) of the LT data (referred to in this article as the "small" data set) on the same unit cell as the RT structure. The crystal class (monoclinic) and space group of the LT phase remain the same as the RT phase, albeit with a different setting (the space group is $P2_1/n$ for the RT phase and $P2_1/c$ for the LT phase). There were a few (generally very weak) reflections which could not be indexed at all using this unit cell and which may be due to satellite crystallites. In addition, the agreement between observed and calculated positions for diffraction maxima based on the orientation matrix was poor for some reflections. This is attributed to the diffuseness of many of the diffraction maxima arising from the orientational disorder.

To ensure the reproducibilty of results, data were collected for one crystal specimen at 123 and 173 K and for a separate specimen at 173 K using laboratory X-ray sources. In view of the large percentage of weak reflections, a data set at 153 K using synchrotron radiation was also obtained. It was hoped that the brighter source would give significantly better results for the weak data, but unfortunately this was not the case. We discuss here only those results obtained at 123 K. The only important differences between the refinements are small variations in the relative disorder populations and differing adp's due to the differing temperatures. Since the disorder populations and the adp's are highly correlated, these differences are probably within experimental error, despite the low standard uncertainties (su's or esd's) as determined from the least-squares process. Table 1 lists the full experimental details for data collection and structure refinement at 123 K. Frames were integrated using the SAINT[25] program, and an absorption correction was deemed unnecessary in view of the small variation in intensities of equivalent reflections. For the synchrotron data, the program SADABS[26] was used to correct for the very substantial beam decay which occurs during data collection.

The LT structure was solved by the direct methods program SHELXS-97[27] using default settings. Essentially all atoms were obtained from this solution, including most of the minor-component disordered Fe atoms. The structure was refined by full-matrix methods using SHELXL-97,[22] against all independent data and with anisotropic thermal parameters for all atoms, except for the minor-component Fe atoms in molecules **3b**. The positional parameters of the minor-component Fe atoms were initially freely refined but in later stages were fixed in a rigid geometry. Occupational parameters for these atoms were refined at all stages. The light atoms were refined with restrained (ISOR) anisotropic thermal parameters, since in an unrestrained refinement several anisotropic thermal parameters became nonpositive definite. In part this problem arises because of the disorder present. The refinement proceeded relatively smoothly, given the large number of data and refined parameters (see Table 1) and given that a substantial portion (∼75%) of the data can be considered unobserved. The largest correlation coefficients involved either the restrained parameters or the minor disordered Fe atom parameters. Importantly, there were no correlation coefficients above 0.5 between metal atoms in different molecules, indicating no serious pseudo-symmetry problems. The largest features were in the vicinity of the Fe atoms in molecules **3b** and **3e**, the most seriously disordered molecules.

Table 2. Selected Bond Lengths (Å) and Bond Angles (deg) for 1

	1a (223 K)	**1b** (223 K)	**1a** (298 K)	**1b** (298 K)
	Distances			
Fe1−Ru1	2.735(1)	2.736(1)	2.735(2)	2.733(2)
Fe2−Ru1	2.734(1)	2.733(1)	2.737(2)	2.730(2)
Fe1−Fe2	2.579(1)	2.575(1)	2.584(2)	2.583(2)
Ru1−C1	1.928(7)	1.942(7)	1.970(10)	1.902(10)
Ru1−C2	1.939(7)	1.920(7)	1.956(10)	1.890(9)
Ru1−C3	1.967(6)	1.943(6)	1.970(8)	1.929(8)
Ru1−C4	1.950(6)	1.935(6)	1.929(8)	1.925(9)
Fe1−C5	1.811(7)	1.779(7)	1.799(10)	1.816(9)
Fe1−C6	1.817(7)	1.800(7)	1.856(9)	1.802(9)
Fe1−C7	1.789(7)	1.805(7)	1.755(10)	1.791(10)
Fe1−C11	1.964(6)	1.940(6)	2.008(8)	1.980(9)
Fe1−C12	2.049(6)	2.147(6)	2.064(10)	2.214(9)
Fe2−C8	1.788(7)	1.806(6)	1.762(10)	1.814(9)
Fe2−C9	1.792(7)	1.806(6)	1.821(11)	1.797(10)
Fe2−C10	1.814(7)	1.822(7)	1.812(11)	1.820(12)
Fe2−C11	2.052(6)	2.124(6)	2.072(8)	2.201(9)
Fe2−C12	1.981(6)	1.943(6)	2.014(9)	1.989(8)
C−O(terminal, mean)	1.128	1.132	1.111	1.132
C −O(bridge, mean)	1.148	1.136	1.136	1.117
	Angles			
Ru−C−O(mean)	177.4	176.6	174.8	176.1
Fe−C−O (terminal,mean)	177.5	176.9	174.6	175.8
Fe1−C11−O11	142.9(5)	146.5(5)	143.1(8)	148.0(8)
Fe1−C12−O12	137.5(5)	135.2(5)	139.7(8)	135.7(7)
Fe2−C11−O11	137.2(5)	134.7(5)	138.3(7)	137.4(7)
Fe2−C12−O12	142.9(6)	146.9(5)	141.6(8)	147.0(7)

Results and Discussion

Structure of $Fe_2Ru(CO)_{12}$ (1). IR spectroscopic[17,28] and Mössbauer[29] studies on cluster **1** indicated that it had a similar structure similar to that of $Fe_3(CO)_{12}$. The substitution derivatives $Fe_2Ru(CO)_{11}(L)$ (L = PPh_3 (**4**), $P(OMe)_3$ (**5**)) were shown to possess two bridging carbonyls about the Fe−Fe bond.[30] Herein we demonstrate that the parent cluster **1** has the same $Fe_3(CO)_{12}$ type structure, with two bridging carbonyls spanning the Fe−Fe edge.

Below 323 K, **1** is isomorphous and isostructural with the osmium analogue $Fe_2Os(CO)_{12}$.[9,31] It crystallizes in the noncentrosymmetric space group *Pn*, with two independent molecules **1a** and **1b**, both of which show a partial, temperature-dependent, "Star of David" disorder in the metal atom positions. Table 2 lists the important metrical parameters for both independent molecules **1a** and **1b** for the more accurate studies at 223 and 298 K, and Figures1 and 2 show ORTEP plots of **1a** and **1b**, respectively, at 233 K. The essential features are very similar to those previously reported for $Fe_2Os(CO)_{12}$.[9,31] The overall molecular structure closely approximates to C_{2v} with the Fe−Fe vector being spanned by two approximately symmetrical carbonyl

(25) SAINT: Area-Detector Integration Software; Siemens Industrial Automation, Inc., Madison, WI, 1995.
(26) SADABS: Area-Detector Absorption Correction; Siemens Industrial Automation, Inc., Madison, WI, 1996.
(27) Sheldrick, G. M. SHELXS-97 (release 97-2); Institüt für Anorganische Chemie der Universität, Tammanstrasse 4, D-3400 Göttingen, Germany, 1998.

(28) (a) Dobos, S.; Nunziante-Cesaro, S.; Maltese, M. *Inorg. Chim. Acta* **1986**, *113*, 167. (b) Knight, J. A.; Mays, M. J. *Chem. Ind.* **1968**, 1159. (c) Shojaie, R.; Atwood, J. D. *Inorg. Chem.* **1987**, *26*, 2199.
(29) Collins, M. P.; Spalding, T. R.; Deeney, F. T.; Longoni, G.; Della Pergola, R.; Venäläinen, T. *J. Organomet. Chem.* **1986**, *317*, 243.
(30) Venäläinen, T.; Pakkanen, T. *J. Organomet. Chem.* **1984**, *266*, 269.
(31) Churchill, M. R.; Fettinger, J. C. *Organometallics* **1990**, *9*, 446.

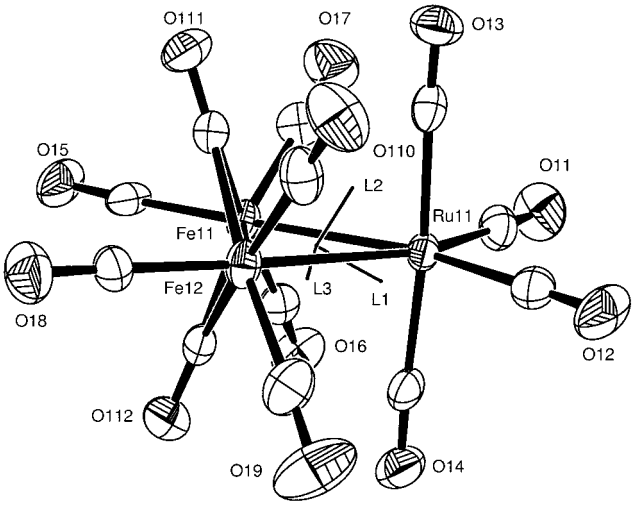

Figure 1. Molecular structure and atomic labeling scheme for the $Fe_2Ru(CO)_{12}$ molecule **1a** at 233 K. Thermal ellipsoids are shown at the 50% probability level.

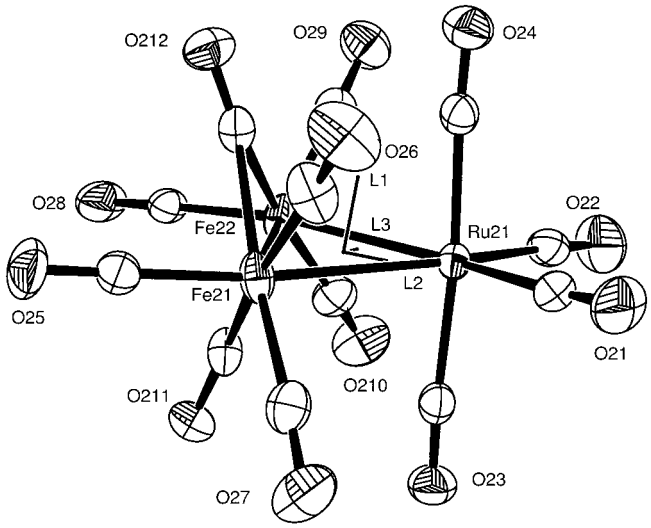

Figure 2. Molecular structure and atomic labeling scheme for the $Fe_2Ru(CO)_{12}$ molecule **1b** at 233 K. Thermal ellipsoids are shown at the 50% probability level.

bridges. However, both **1a** and **1b** show small distortions toward C_2 symmetry, especially the latter molecule. The two molecules are nearly, but not exactly, related to each other by an inversion center, as has been discussed in some detail for $Fe_2Os(CO)_{12}$ by Churchill and Fettinger.[31]

At 223 K the structure is perfectly ordered, and raising the temperature causes an increasing Star of David disorder in the metal atom positions, with mean population ratios for both molecules of 0.89:0.11 at 298 K and 0.71:0.29 at 313 K. Heating the crystal sample at 323 K induces a phase change to the centrosymmetric space group $P2_1/n$, whereby the structure becomes isostructural and isomorphous with the room-temperature phase of $Fe_3(CO)_{12}$. The asymmetric unit now consists of one half-occupancy molecule of **1** situated on the crystallographic inversion center at the origin, with an exact 0.5:0.5 disorder in the metal atoms. All these changes are completely reversible and hence dynamic in nature. We have previously reported[9] that $Fe_2Os(CO)_{12}$ undergoes an apparently similar phase change. The transition temperature (~373 K) was significantly

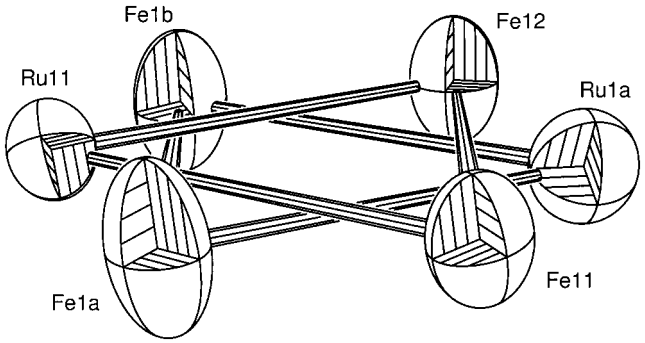

Figure 3. The Star of David orientation of the two Fe_2Ru triangles for molecule **1a** at 298 K. Thermal ellipsoids are drawn at the 50% probability level.

higher, which precluded data collection due to rapid crystal decomposition.

Figure 3 shows the Star of David orientation of the two Fe_2Ru triangles for molecule **1a** at 298 K. The dynamic disorder requires that the metal atoms *effectively* rotate by 180° about the triangular pseudo 3-fold axis. In all the studies reported in this paper, we found no evidence for any Fe/Ru disorder at individual metal sites, though this is difficult to rule out completely. While the structural evidence for **1** does not offer any direct insight into the pathway involved, it seems unlikely that this rotation is accomplished in a single step. In line with the evidence obtained from $Fe_2Os(CO)_{12}$[9] and **2** (see below), we suggest it occurs in 60° steps, with the residence time and populations of the intermediate orientations being small compared with those of the observed orientations. We note that the adp's of the Fe atoms show the same feature previously noted[2k,3h] in the RT structure of $Fe_3(CO)_{12}$ (see below for further comments) and that of $Fe_2Os(CO)_{12}$,[9,31] namely that the vibrational component normal to the metal plane is greater than in the other directions (see Figures 1−3). This is manifest in the magnitude of U_{22}, which is about twice the magnitude of either U_{11} or U_{33} (the metal triangles of both **1a** and **1b** lie approximately normal to the crystallographic *b* axis). These adp's have been cited[2k,3h,11,13] as supporting evidence for proposed fluxional mechanisms.

Molecules **1a** and **1b** are very similar, even to the extent of their anisotropic displacement parameters, as is clear from Table 2 and Figures 1 and 2. The analysis of **1** at 233 K represents the best available data on the $Fe_3(CO)_{12}$ structural archetype, since the crystal quality was high and no disorder is present. Moreover, we have two chemically identical but crystallographically independent molecules, and a detailed comparison is illuminating. The metal skeletons are identical within experimental error, while the relationship between the carbonyl ligand polytopes of both molecules is most easily appreciated when the two molecules are superimposed, as shown in Figure 4. In this view, the metal triangles of both molecules have been fitted by least-squares methods to minimize their positional differences (RMS misfit 0.002 Å). We define the term *distortion coordinate* to signify the set of displacement vectors which relate corresponding pairs of atoms in the two superimposed molecules. Since **1a** and **1b** are chemically identical and only differ in the packing forces they experience, this distortion coordinate represents a soft-

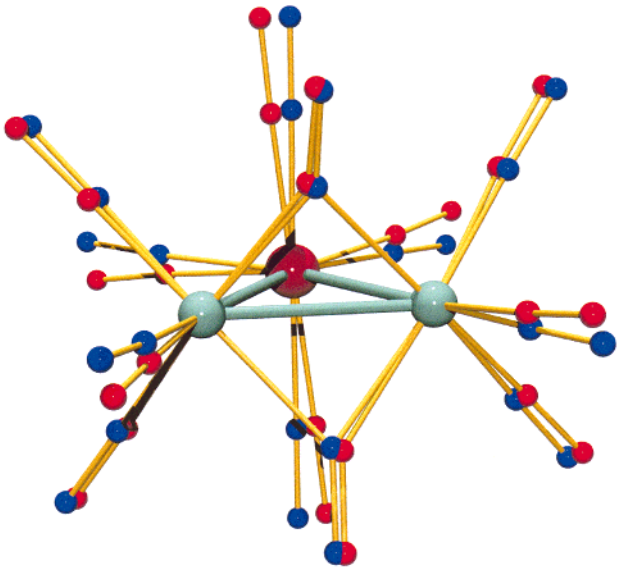

Figure 4. Superimposition view of molecules **1a** (blue) and **1b** (red) at 233 K. The Fe and Ru atoms are in common.

mode motion of the CO ligands relative to the metal skeleton. The oxygen atoms show greater average displacements than the carbon atoms and thus provide a clearer picture of the distortion coordinate. The largest O atom displacements are ~0.5 Å (associated with the equatorial CO ligands on the Ru atom), while the mean displacement of the O atoms is 0.29 Å. This latter value corresponds to a mean-square displacement of 0.08 Å^2, which is entirely consistent with the magnitudes of the U_{ij} tensors.

The light-atom adp's in the structural analysis at 223 K are unbiased by the effects of disorder, and in the absence of contamination from charge-density contributions, absorption, or other systematic errors, they ought to reflect this soft mode. In a qualitative sense, this appears to be the case. In particular, the four chemically equivalent pseudoaxial carbonyls on the two Fe atoms (carbonyls 6, 7, 9, and 10, Figures 1 and 2) show their greatest thermal motion approximately normal to their mean plane, which is also the direction of the displacement vectors for these same CO ligands in the distortion coordinate shown in Figure 4. A useful criterion to ascertain whether the measured adp's represent genuine vibrational motion is the Hirshfeld rigid bond postulate.[32] This states that, for a pair of covalently bonded atoms, the mean-square displacement amplitudes of both atoms along the bond vector should be equal. For atoms as least as heavy as carbon the difference $\Delta(z^2_{A,B})$ should normally[32] be below 0.001 Å^2. For molecules **1a** and **1b** the mean $\Delta(z^2_{A,B})$ value between bonded C and O atoms was ~0.008 Å^2 with a standard uncertainty (su) of ~0.005 Å^2. The experimental error on the adp's thus precludes a meaningful interpretation of the Hirshfeld rigid bond postulate for this system, but within error they are close to zero.

A TLS analysis[33] of the adp's using the program THMA11[34] has been undertaken. The U_{ij} values were determined from a refinement using all data, as applying a cutoff of $(\sin\theta)/\lambda \geq 0.15$ did not make a significant difference. The first model investigated was the full rigid-body treatment. Figures 1 and 2 show the directions of the principal axes of the libration tensor, and Table 3 lists the eigenvalues and eigenvectors of **L** and **T** in the inertial frame. The translation tensor **T** is approximately isotropic, while the rigid-body libration is primarily about the axes L1 and L2, which lie approximately along the pseudo-C_3 axis of the metal triangle and the molecular C_2 axis. The agreement factors R_w for molecules **1a** and **1b** are 0.137 and 0.183, respectively, which indicates that some residual internal motion is present. This is most clearly demonstrated in the PEANUT[35] plot (Figure 5), which shows the RMS displacement differences between the observed and rigid-body calculated adp's for molecule **1a**. The PEANUT plot for molecule **1b** is very similar. Most differences are positive; therefore, an *excess* thermal motion is indicated. The residual motion of the metal atoms is virtually zero, primarily because the rigid-body calculation is weighted in favor of the heavier atoms. Figure 5 thus provides, to a first approximation at least, a graphical display of *the residual motion of the carbonyl ligands about the rigid metal framework*. This residual motion is reasonably consistent with the displacement vectors shown in Figure 4.

We have also analyzed the thermal motion in **1** in terms of the proposed models for the fluxional behavior in $M_3(CO)_{12}$ clusters. In one model the whole carbonyl polytope (one bridging C atom was not included to avoid a singularity) was treated as an attached rigid group undergoing libration about the axis containing the Ru atom and the midpoint of the Fe−Fe bond (the Johnson[2j−m,10] C_2 libration). In a second model the whole carbonyl polytope was treated as an attached rigid group

Table 3. Eigenvectors and Eigenvalues of the T and L Tensors in the Inertial Frame, from the Rigid-body TLS Analysis on 1 at 223 K

	ξ(1)	ξ(2)	ξ(3)	RMS (Å)	RMS (deg)	R_w[a]
			Molecule **1a**			
L tensor	0.899 45	0.060 1	0.431 70		3.27	0.137
	0.400 87	0.265 05	−0.876 96		3.21	
	−0.174 07	0.961 83	0.211 13		1.60	
T tensor	0.197 66	−0.203 83	−0.958 84	0.173		
	−0.515 91	0.810 09	−0.278 56	0.148		
	0.833 35	0.549 74	0.054 97	0.139		
			Molecule **1b**			
L tensor	−0.115 37	0.246 96	−0.962 13		3.15	0.183
	−0.987 88	−0.129 83	0.085 13		2.88	
	−0.103 89	0.960 29	0.258 94		1.28	
T tensor	−0.017 35	0.075 39	−0.997 00	0.179		
	−0.759 52	0.647 5	0.062 18	0.139		
	0.650 3	0.758 33	0.046 03	0.132		

[a] $R_w = [\Sigma(w\Delta U)^2/\Sigma(wU)^2]^{1/2}$.

(32) Hirshfeld, F. L. *Acta Crystallogr. Sect. A* **1976**, *A32*, 239.

(33) The TLS approach analyzes the experimentally determined anisotropic displacement parameters (adp's) in terms of a rigid-body motion (with possibly some internal motion) of the molecule. This motion is described in terms of a translation tensor **T**, a libration tensor **L**, and a tensor **S** which accounts for the correlation between **T** and **L.** For an excellent introduction to this topic, see: Dunitz, J. D. In *X-ray Analysis of the Structures of Organic Molecules*; VCH: Weinheim, Germany, 1995; pp 244−261. See also: (a) Schomaker, V.; Trueblood, K, N. *Acta Crystallogr., Sect. B* **1968**, *B24*, 63. (b) Dunitz, J. D.; Schomaker, V.; Trueblood, K. N. *J. Phys. Chem.* **1988**, *92*, 856. (c) Dunitz, J. D.; Maverick, E. F.; Trueblood, K. N. *Angew. Chem., Int. Ed. Engl.* **1988**, *27*, 880.

(34) Trueblood, K. N. *Acta Crystallogr., Sect. A* **1978**, *A34*, 950.

(35) (a) Hummel, W.; Hauser, J.; Bürgi, H.-B. *J. Mol. Graphics* **1990**, *8*, 214. (b) Hummel, W, Raselli, A.; Bürgi, H.-B. *Acta Crystallogr., Sect. B* **1990**, *B46*, 683.

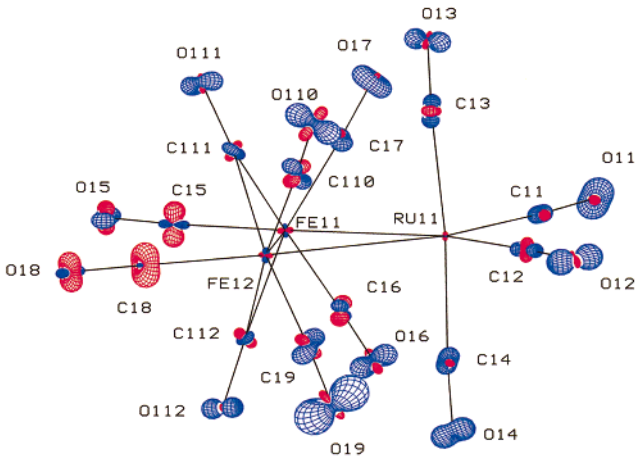

Figure 5. PEANUT plot for molecule **1a** showing the RMS displacement differences between the observed and rigid-body calculated adp's. Positive values are shown in blue and negative values in red.

undergoing libration about an axis containing the trans-related equatorial carbonyl ligands (the Mann[11] S_{10} rotation). Both symmetry-related axes were investigated. For molecule **1a**, the Johnson model gave an R_w value of 0.118, while the Mann models gave R_w values of 0.117 and 0.116. We have similarly examined the fluxional models of Cotton and Troup,[2b] Hanson *et al.*,[2d] and Lentz and Marschall,[2q] and these gave R_w values for molecule **1a** of 0.129, 0.122, and 0.128, respectively. All these agreement indices are essentially identical and do not represent significant improvements over the full rigid-molecule treatment. We therefore find no compelling evidence in favor of any of the proposed mechanisms from the adp's in cluster **1**.

Finally we have examined a model where each $M(CO)_n$ group (the $Ru(CO)_4$ group and the two *fac*-$Fe(CO)_3$ groups) are treated as *isolated rigid* $M(CO)_n$ groups. The bridging carbonyls were not included in the analysis, since they show the least thermal motion, and in any case partitioning them into $M(CO)_n$ groups is necessarily arbitrary. All these isolated groups show significant librations (see Table S1 in the Supporting Information), and the overall mean agreement factor R_w was 0.058 for both **1a** and **1b**. This is a substantial improvement over the rigid-molecule approach and indicates that it may be inappropriate to analyze the thermal motion in metal clusters in terms of this latter model. This approach assumes and allows no correlation between individual $M(CO)_n$ librations and effectively treats the metal cluster as a collection of rigid $M(CO)_n$ groups held together by relatively soft metal−metal interactions.

Since the literature discussion on the fluxional modes[11,13] of $M_3(CO)_{12}$ clusters is often couched in terms of the motion of the metal triangle relative to a (fixed) ligand polytope, we have also examined the differences between the molecules **1a** and **1b** from this viewpoint. The C and O atom positions of **1a** and **1b** were fitted by least-squares minimization. The ligand polytopes are less similar than are the metal triangles and gave an RMS misfit of 0.195 Å. The metal triangle in **1b** was found to be displaced from that of **1a** such that the Ru atoms differed in position by only 0.03 Å, while the two Fe atoms of **1b** were both displaced by 0.09 Å from those in **1a** *one above and one below* the metal plane of **1a**. These positional discrepancies are relatively minor, since the displacement along the soft-mode coordinate as represented by molecules **1a** and **1b** is quite small.

Relationship of the Structure of 1 with Substitution Derivatives. There have been three reported crystal structures of substitution derivatives of **1**, where CO ligands are replaced by other two-electron-donor ligands, namely $Fe_2Ru(CO)_{11}(L)$ (L = PPh_3[30] (**4**), $P(OMe)_3$[30] (**5**)) and $Fe_2Ru(CO)_{10}(Pr^i\text{-PCya})$[36] (**6**). We have compared all three structures with that of **1a** by least-squares fitting of the metal triangle as detailed above. The Fe−Fe distances in **4** (2.575(1) Å) and **5** (2.581(1) Å) are very similar to those in **1**, though the Fe−Ru distances of 2.796(1) and 2.771(1) Å in **4** and 2.766(1) and 2.757(1) Å in **6** are significantly longer than those in **1**. The ligand polytopes of $Fe_2Ru(CO)_{11}(L)$ (L = PPh_3, $P(OMe)_3$) are very similar to each other and to that of **1a**, with no consistent pattern of distortions being observed. The RMS misfit of metal atoms was ~0.03 Å, and the mean discrepancies between O atom positions compared with **1a** were respectively 0.19 and 0.16 Å.

On the other hand, the structures of **1a** and **6**[36] are strikingly different. The latter molecule has a pair of CO ligands bridging an Fe−Ru edge, with the two N-donors of the Pr^i-PCya ligand occupying two axial positions on the Ru atom. The relationship between the ligand polytopes, corresponding to the movement of the pair of bridging carbonyls from one edge to an adjacent one, is very similar to that discussed below in more detail for $Fe_3(CO)_{12}$ (see Figure 11).

Structure of $FeRu_2(CO)_{12}$ (2). The IR spectra[17,28c] of **2** indicate it has an all-terminal CO arrangement, while Mössbauer studies[29] and the crystal structures of $FeRu_2(CO)_{11}(PPh_3)$ and $FeRu_2(CO)_{10}(PPh_3)_2$ reported by Venäläinen and Pakkanen[30] suggest a D_3 distortion. These authors also described[30] a room-temperature unit cell for **2**, with similar metrical parameters and the same space group as ourselves, but were unable to resolve the disorder. In our own hands, we found the centrosymmetric phase difficult to solve by standard Patterson or direct methods. The breakthrough came with a correct lucky guess that the metal triangle was situated on an inversion center.

At 173 K, crystals of cluster **2** exhibit the noncentrosymmetric space group *C*2cb, with no trace of disorder in the metal framework. An ORTEP view shown in Figure 6 illustrates the molecular structure, while important metrical parameters are given in Table 4. The all-terminal carbonyl arrangement is closely related to that found in several phosphine and phosphite derivatives of $M_3(CO)_{12}$ (M = Fe,[37] Ru,[7] Os[7]). The overall ligand polytope is approximately icosahedral, and the disposition of the metal triangle within this leads to a D_3 distorted molecule, though the actual symmetry of **2** is close to idealized C_2 due to asymmetry of the metal

(36) Kraakman, M. J. A.; Elsevier: C. J.; Ernsting, J.-M.; Vrieze, K.; Goubitz, K. *Inorg. Chim. Acta* **1993**, *203*, 129.
(37) Adams, H.; Chen, X.; Mann, B. E. *J. Chem. Soc., Dalton Trans.* **1996**, 2159.

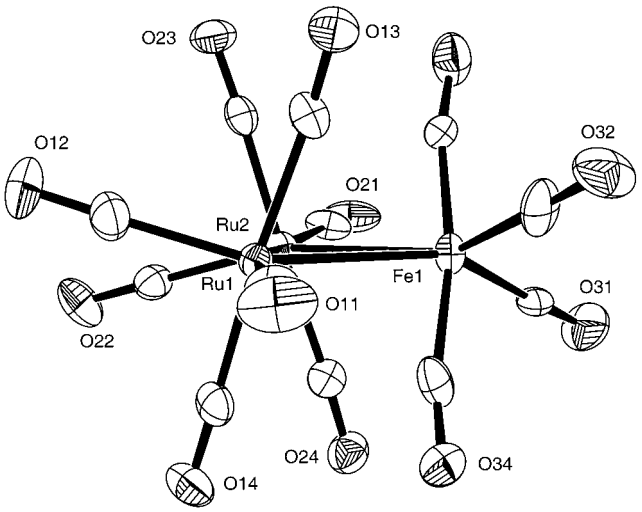

Figure 6. Molecular structure and atomic labeling scheme for $FeRu_2(CO)_{12}$ (**2**) at 173 K. Thermal ellipsoids are shown at the 50% probability level.

Table 4. Selected Bond Lengths (Å) and Bond Angles (deg) for 2 at 173 K

Bond Lengths			
Fe1−Ru1	2.775(2)	Ru2−C24	1.968(12)
Fe1−Ru2	2.762(2)	Fe1−C31	1.822(12)
Ru1−Ru2	2.806(1)	Fe1−C32	1.749(13)
Ru1−C11	1.947(13)	Fe1−C33	1.826(12)
Ru1−C12	1.917(11)	Fe1−C34	1.825(14)
Ru1−C13	1.956(12)	Ru1···C34	2.800(12)
Ru1−C14	1.968(11)	Ru2···C33	2.811(12)
Ru2−C21	1.950(14)	Fe1···C24	2.946(12)
Ru2−C22	1.923(10)	Fe1···C13	2.888(12)
Ru2−C23	1.935(11)	C−O (*mean*)	1.132

Bond Angles			
Ru1−C13−O13	171.7(11)	Fe1−C33−O33	168.9(9)
Ru2−C24−O24	173.8(11)	Fe1−C34−O34	169.4(10)
remaining Ru−C−O (mean)	177.5	remaining Fe−C−O (mean)	177.8

triangle. The D_3 configuration for $M_3(CO)_{12}$ clusters is central to the Johnson proposal[2j−m,10] for their fluxionality, and molecular mechanical calculations by Lauher[38] and more recently by Sironi[39a] have indicated this is a very favorable geometry. Indeed, it is predicted[39a] to be the most stable configuration for all three molecules $M_3(CO)_{12}$ (M = Fe, Ru, Os), in contradiction to their experimentally observed structures. Complex **2** is the first crystallographically characterized example of a homoleptic $M_3(CO)_{12}$ cluster with this D_3 geometry.

One way of viewing the D_3 structure is to consider it as arising from the D_{3h} structure of the parent $M_3(CO)_{12}$ (M = Ru,[40] Os[41]), whereby each $M(CO)_4$ fragment is tilted *in the same direction* about the fragment C_2 axis, usually by ∼20°. There are some minor differences between the structure of **2** and "classical" D_3 distorted clusters as exemplified by $Ru_3(CO)_9(PMe_3)_3$.[7e] The *mean* value of the torsion angles M1−M2−M3−C(ax) for the two pseudoaxial carbonyls on the metal atoms Fe(1), Ru(1), and Ru(2) are respectively 65.8°, 72.3°, and 74.1°. This shows that the $Fe(CO)_4$ group is significantly more skewed relative to the metal triangle than the two $Ru(CO)_4$ groups. Moreover, the pair of equatorial carbonyls trans to the Ru−Ru bond, CO(11) and CO(21), are virtually coplanar with the metal triangle, in contrast with the remaining equatorial ligands, which lie significantly out of this plane. The equatorial carbonyl ligands do not deviate significantly from linearity (*mean* M−C−O angle 178.0°), but the axial carbonyls, especially those on Fe(1), show a small deviation toward a semibridging character (see Table 4).

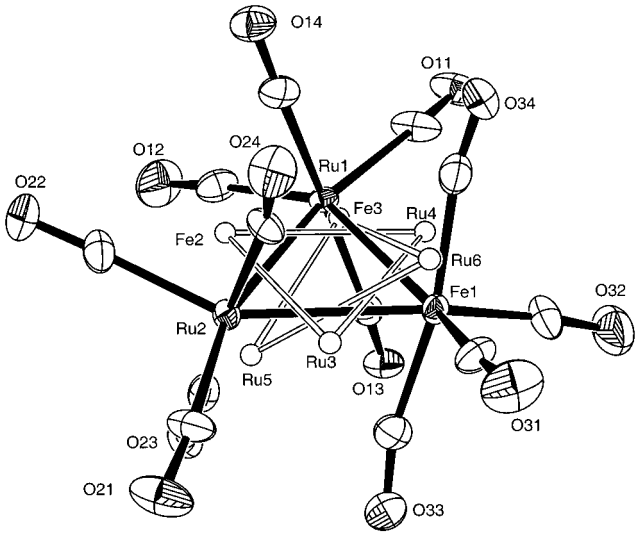

Figure 7. Molecular structure and atomic labeling scheme for $FeRu_2(CO)_{12}$ (**2**) at 223 K, showing the disordered metal positions. Thermal ellipsoids are shown at the 50% probability level; disordered atoms are shown as spheres with arbitary radius.

When crystals of **2** are warmed from 173 to ∼230 K, there is an increase in the disorder in the metal triangle, while the same space group is retained. Several data sets were collected in this temperature range (see Experimental Section), but we discuss in detail here only the data set collected at 223 K. The molecular structure is essentially the same as observed at 173 K, but two extra disordered positions of the $FeRu_2$ triangle were observed. An ORTEP view is shown in Figure 7. The extra orientations of the triangle were refined as rigid groups, using the geometry found in the major component. The refined populations of the three orientations were 0.858:0.095:0.047, and only the major positions of the light atoms were determined. While one of the triangles (Fe2−Ru3−Ru4) lies in the plane of the major component and is rotated by 180° about the molecular pseudo-C_3 axis (as is observed in other examples such as $Fe_2Os(CO)_{12}$[9,31] and $Fe_2Ru(CO)_{12}$—see above), the other component (Fe3−Ru4−Ru5) lies substantially out of the plane. The position of this latter triangle suggests that the effective 180° rotation proceeds in steps involving significant out-of-plane displacements.

These observations are compounded by the high-temperature phase of **2**. Above ∼230 K, a phase transition to the centrosymmetric space group *Ccmb* occurs. The reason for the phase change is attributed solely to the orientational disorder of the metal atoms. The

(38) Lauher, J. W. *J. Am. Chem. Soc.* **1986**, *108*, 1521.
(39) (a) Sironi, A. *Inorg. Chem.* **1996**, *35*, 1725. (b) Sironi, A. *Inorg. Chem.* **1995**, *34*, 1342.
(40) (a) Mason, R.; Rae, A. I. M. *J. Chem. Soc., Dalton Trans.* **1968**, 778. (b) Churchill, M. R.; Hollander, F. J.; Hutchinson, J. P. *Inorg. Chem.* **1977**, *16*, 2655. (c) Braga, D.; Grepioni, F.; Tedesco, E.; Dyson, P. J.; Martin, C. M.; Johnson, B. F. G. *Transition Met. Chem.* **1995**, *20*, 615.
(41) (a) Corey, E. R.; Dahl, L. F. *Inorg. Chem.* **1962**, *1*, 521. (b) Churchill, M. R.; DeBoer, B. G. *Inorg. Chem.* **1977**, *16*, 878.

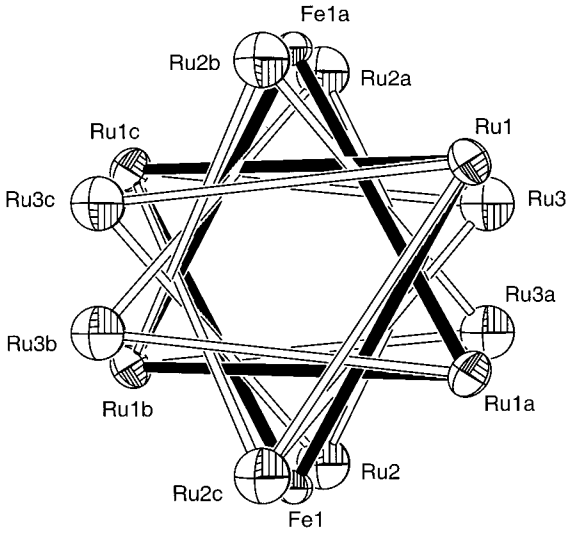

Figure 8. View of the disordered metal framework of $FeRu_2(CO)_{12}$ (**2**) at 291 K. Atom labels ending with "a" correspond to the symmetry operation $x, -y, z$, those with "b" to $-x, -y, -z$, and those with "c" to $-x, y, -z$.

carbonyl polytope of **2** is approximately icosahedral and has an inversion center which is almost crystallographically exact. The addition of this inversion center to the polytope in the noncentric *C*2*cb* phase together with the application of the appropriate translation allows the transformation to the centric space group *Ccmb*. In other words, the carbonyl ligand packing in the two phases is almost exactly the same, the only difference being the degree of metal atom disorder. The centrosymmetric phase is seriously disordered with respect to the metal atom positions, which show an extended Star of David disorder. The *molecular* structure can only be ascertained approximately, and it is similar to that of **2** at 173 K. Figure 8 shows an ORTEP view of the metal atom disorder. There are two equally populated "major" positions (total population 81.4(7)% at 291 K and 87.9(7)% at 243 K) and four equally populated "minor" positions. The crystallographic site symmetry is 2/*m*, which is higher than the inversion symmetry found for $Fe_3(CO)_{12}$ in the room-temperature phase[2a,b] and accounts for the greater disorder in **2**. Figure 8 shows in detail the 60° steps required to interconvert the two "major" orientations of the metal triangle in the crystal. The position of the Fe atom in these intermediate orientations was too close to the Ru1 atom to be distinguishable in the X-ray experiment, and they were set to be identical in the refinements. Due to the relatively high errors on the adp's for the ordered structure at 173 K, a TLS analysis of the thermal motion was not undertaken. Even a cursory glance at Figure 6 shows that some carbonyl groups break the Hirshfeld rigid-bond criterion quite markedly.

Relationship of the Structure of 2 with Substitution Derivatives. The structures of two substitution derivatives of **2** have been reported,[30] namely $FeRu_2(CO)_{12-n}(PPh_3)_n$ ($n = 1$, **7**; and $n = 2$, **8**). The basic structures are similar to that of **2**, but they show small differences of importance in the context of this article. The Ru−Ru distances in **7** and **8** (2.827(1) and 2.854(2) Å, respectively) are slightly longer than those found in the parent **2** (Table 4). The Fe−Ru distances in **7** (2.788(1) and 2.796(1) Å) are longer than in **2**, while that in **8** (2.664(2) Å) is noticeably shorter than in **2**. These differences may be related to the degree of semibridging character of the axial carbonyls of the $Fe(CO)_4$ and $Ru(CO)_4$ groups. In **7** one Fe−Ru edge has an incipient pair of CO bridges (Fe···C = 2.730 Å, Ru···C = 2.582 Å), this being the longest Fe−Ru vector. In contrast, in **8** both Fe−Ru edges are identical by symmetry, and the semibridging interaction is somewhat greater (Ru···C = 2.522 Å, Fe···C = 2.679 Å), leading to shorter Fe−Ru distances. As found in **2**, the pair of equatorial ligands trans to the Ru−Ru bond in both **7** and **8** are nearly coplanar with the metal triangle, while the other equatorial ligands are displaced out of this plane.

Low-Temperature (LT) Phase of $Fe_3(CO)_{12}$. Cooling crystalline samples of $Fe_3(CO)_{12}$ **3** below ~210 K causes a phase transition to a new low-temperature (LT) monoclinic phase. There is significant diffuse scattering, especially along the layer lines, which is indicative[42] of continuing disorder in this new phase. As indicated in the Experimental Section, the LT phase is a supercell of the RT phase with a unit cell 9 times the volume. The asymmetric unit comprises five independent molecules of $Fe_3(CO)_{12}$, **3a**−**e**, one of which (**3e**) is a half-molecule situated about the inversion center at the origin. The disorder exhibited by **3e** is thus similar to that observed in the RT phase, but it was not possible to deconvolute the separate positions of the 12 carbonyl ligands in the present study. The structural model for **3e** thus consists of three half-occupancy Fe atoms and six full-occupancy C and O atoms. The adp's for these C and O atoms are significantly larger than for the other four molecules, undoubtedly reflecting the convolution of two close atomic sites into the adp.

The other four complete molecules of $Fe_3(CO)_{12}$ are situated in general positions, so that no disorder is *required* by crystallographic site symmetry. Nevertheless, three of these molecules, **3b**−**d**, show the typical Star of David disorder in the metal atom positions. The fourth molecule, **3a**, showed no detectable disorder, thus providing the first structural analysis on a *completely ordered* molecule of $Fe_3(CO)_{12}$. For **3b**−**d**, respectively, the proportions of the major components are 0.822(3), 0.703(2), and 0.652(2) at 123 K, changing slightly to 0.778(3), 0.675(3), and 0.618(2) at 173 K. For all these molecules, only the major positions of the 12 C and O atoms could be observed and refined, and the light atom adp's in **3b**−**d** therefore subsume any disorder. The important geometrical parameters for **3a**−**d** are given in Table 5, while an ORTEP plot for molecule **3a** is shown in Figure 9.

From Table 5 the following general conclusions may be drawn.

(a) Molecules **3a**, **3c**, and **3d** are very similar to each other. They all have close to idealized C_{2v} symmetry. The CO bridges are essentially symmetrical, as can be ascertained both from the Fe−C distances and from the Fe−C−O angles, which span the small range 137.7(7)−144.1(9)°. As we have noted previously,[15] the bridge asymmetry seen in the room-temperature structure[2b] is almost certainly an artifact of the anisotropic refinement. The bridged Fe−Fe bond is identical within error in all three molecules, mean 2.552(2) Å, while the nonbridged distances show only a marginally greater

(42) Welberry, T. R.; Butler, B. D. *Chem. Rev.* **1995**, *95*, 2369.

Table 5. Selected Bond Lengths (Å) and Bond Angles for the Four Molecules of $Fe_3(CO)_{12}$ in General Positions at 123 K[a]

	3a	3b	3c	3d
		Bond Distances		
Fe1−Fe2	2.698(2)	2.646(2)	2.690(2)	2.695(2)
Fe1−Fe3	2.680(2)	2.682(2)	2.698(2)	2.683(2)
Fe2−Fe3	2.553(2)	2.551(2)	2.549(2)	2.554(2)
Fe2−C1	2.003(9)	2.215(11)	2.051(11)	2.002(10)
Fe3−C1	1.955(10)	1.906(11)	2.099(11)	2.080(10)
Fe2−C2	1.944(9)	1.933(12)	2.041(11)	2.106(11)
Fe3−C2	1.992(9)	2.313(12)	1.987(10)	2.090(11)
		Bond Angles		
Fe2−C1−O1	139.6(8)	134.0(9)	144.1(9)	141.9(8)
Fe3−C1−O1	140.0(8)	149.9(10)	140.1(9)	140.2(8)
Fe2−C2−O2	141.4(7)	151.4(10)	139.2(8)	144.0(8)
Fe3−C2−O2	137.7(7)	134.7(9)	142.3(8)	140.8(9)

[a] The numbering scheme is the same for all four molecules, with the first digit of each atom number indicating the molecule; i.e., the distance Fe1−Fe2 corresponds to Fe11−Fe12 in molecule **3a**, Fe21−Fe22 in molecule **3b,** etc.

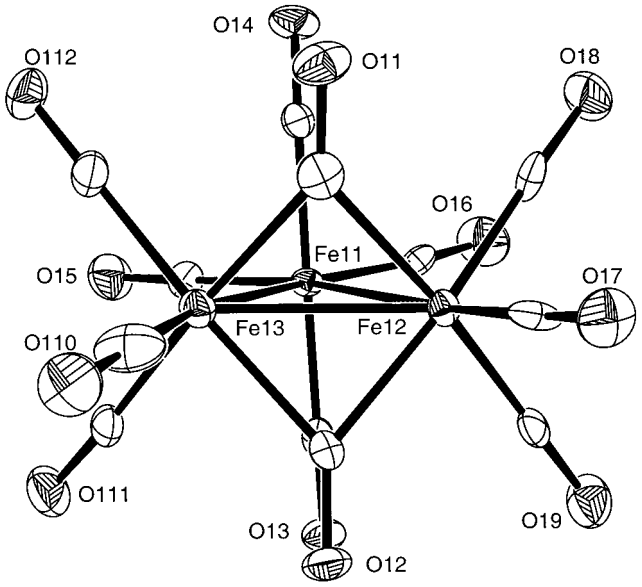

Figure 9. Molecular structure and atomic labeling scheme for the $Fe_3(CO)_{12}$ molecule **3a** at 123 K. Thermal ellipsoids are shown at the 50% probability level.

variation: 2.680(2)−2.698(2) Å, mean 2.691 Å. Molecule **3a** provides light-atom positions which are unbiased by the effects of disorder. The terminal carbonyls are closer to linearity (the range of Fe−C−O angles is 171.9(9)−178.2(8)°, mean 175.5°) than for molecules **3c** or **3d** (the mean Fe−C−O angle is 172.7° for molecule **3c** and 167.9° for molecule **3d**).

(b) Molecule **3b** shows a more distorted C_2 geometry, with distinctly asymmetric bridging carbonyls, Δ(Fe−C) ≈ 0.3 Å. The bridged Fe−Fe distance is identical with that found in the other molecules, while one of the nonbridged distances, Fe21−Fe22, is significantly shorter than the other. However, this is almost certainly an artifact, since the Fe atoms have very unusual thermal parameters. This undoubtedly represents further unresolved disorder, but despite several attempts, no more satisfactory a model could be obtained for molecule **3b**. The resultant geometry must be viewed with caution.

As for **1** and **2**, the underlying reason for this phase transition must be sought in the orientational disorder in the metal triangles, since the packing of the CO ligands is very similar in both phases. The unit cell packing diagram in Figure 10 illustrates the orientation of the metal triangles. Molecule **3e** lies at the origin, and the relationship between the RT cell and the new supercell is most obvious from the *bc* plane. Two molecules, **3d** and **3e**, straddle this plane, and if molecule **3d** were to acquire the same 50:50 metal disorder (and hence a new inversion center) as is found for molecule **3e**, then the repeat distance along the *b* axis would become one-third of the observed repeat distance (i.e. the actual RT *b* axial length). It is important to emphasize that, apart from the one-third translation along the *b* axis, the orientations of the metal atoms in molecules **3d** and **3e** relative to the crystallographic axes are almost precisely the same. The relationship between the supercell and the RT unit cell is thus very close, as is clearly indicated by the diffraction pattern. Moreover, the presence of layers of metal triangles at one-third and two-thirds along the *b* axis is manifest in the intensities of the 0*k*0 reflections, which shows systematic weaknesses for $k \neq 3n$ as well as absences for $k \neq 2n$.

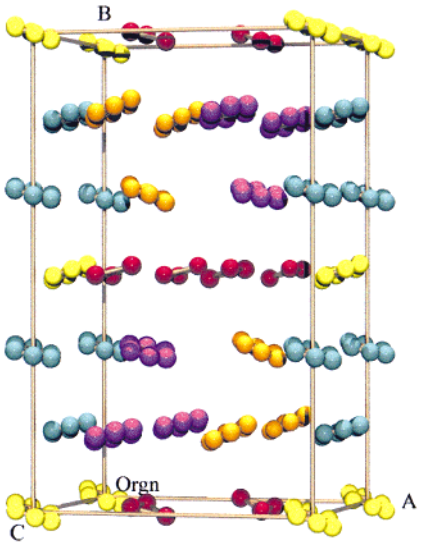

Figure 10. Unit cell packing diagram of **3** at 123 K showing only the Fe atoms of molecules **3a** (red), **3b** (orange), **3c** (violet), **3d** (green), and **3e** (yellow).

The change in diffraction pattern is entirely reversible, and we estimate the phase transition occurs around 210(±10) K. This study therefore provides categorical proof that the disorder in $Fe_3(CO)_{12}$ is dynamic in origin. Moreover, in the solid state at least, we have strong evidence for an *effective rotation* of the Fe_3 triangle within a relatively rigid carbonyl framework, such a movement being required to account for the phase change. Our studies are also entirely in keeping with the solid-state ^{13}C NMR studies of Hanson et al.,[2d] which show that at RT there are effectively six independent crystallographic environments for the carbonyl ligands, while at lower temperatures there are a greater number of independent environments. At room temperature, the Fe_3 triangles must be moving between the two centrosymmetrically related sites at a rate which is rapid compared with the NMR time scale. However, the *pathway* taken by the Fe atoms is not delineated, either by the crystallographic or by the NMR data.

The "Small" Data Set. In addition to the above analysis on the full data set, a subset (one-ninth) of the data could also be indexed using the same unit cell as at room temperature. About 70% of the total scattering from the full data set is concentrated in this "small" data set, and these data were analyzed in order to understand the relationship between the two phases of $Fe_3(CO)_{12}$. The results[43] clearly show that the structural information derived from the "small" data set of the LT phase is identical with that obtained from the RT phase. Nevertheless, it is equally obvious that any description of the crystal and molecular structure of $Fe_3(CO)_{12}$ based on analysis of the "small" data set, or our original[2c] 100 K data set, is incomplete and represents only an "average" of the true structure. We find it disturbing that, by all the commonly accepted crystallographic criteria (i.e. low R_F values and electron density residuals, acceptable thermal parameters, and chemical sensibility of the model), there appears to be no fault with this erroneous partial model. The weak reflections arising from the supercell were not noticed in our original study,[2c] and this work clearly illustrates a major advantage of area detectors over serial detectors when phase changes occur.

Comments on the Fluxionality in $Fe_3(CO)_{12}$. Our new results on **3** cast considerable doubt on the interpretation of the Fe atom adp's associated with the CO-bridged edge,[2c,k,3h] in relation to the fluxional behavior of $Fe_3(CO)_{12}$. In particular, from the analysis[43] of the "small" data set, we find exactly the same elongation normal to the Fe_3 plane (U_{22} is about twice the value of U_{11} and U_{33}) as in the previous RT study,[2b] and in our previous study at 100 K.[2c] Since, for the "small" data set at least, these adp's without question represent an averaging over the five independent molecules, the previous assumption[2c,k,3h] that they indicate low-amplitude vibrational modes is unsafe and probably unjustified. Further emphasis to this point is seen in Figure 9, where the ordered molecule **3a** shows no evidence for thermal ellipsoid elongation normal to the Fe_3 plane. A recent reinterpretation[2i] of the variable-temperature ^{57}Fe Mössbauer spectrum of $Fe_3(CO)_{12}$ was based on our earlier[2c] erroneous thermal parameter data and may have to be reassessed in the light of the new results presented here.

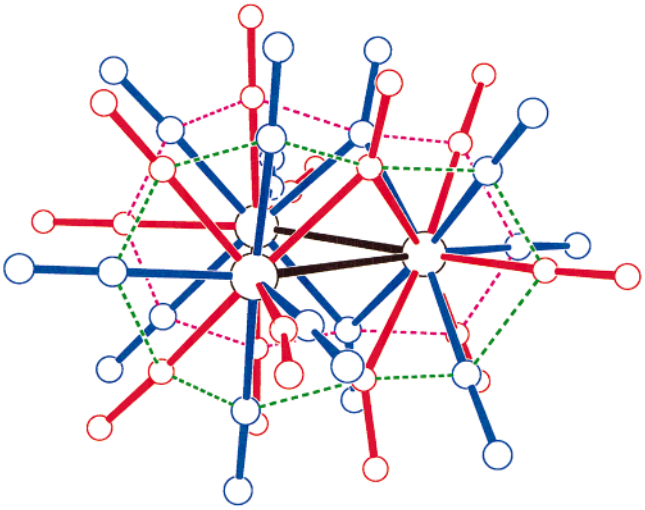

Figure 11. Superimposition view of two molecules of $Fe_3(CO)_{12}$ (shown in red and blue), with the bridging carbonyls on different edges. The Fe atoms are common to both structures.

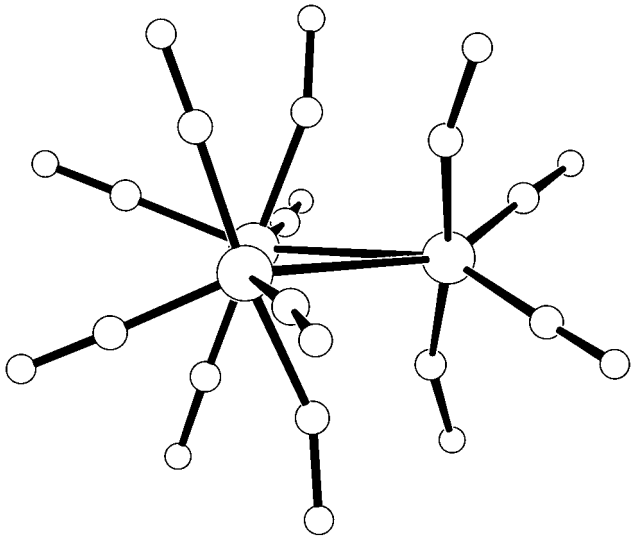

Figure 12. Proposed intermediate in the lowest energy fluxional exchange in $Fe_3(CO)_{12}$.

We also wish to comment on the fluxional behavior of **3** from a structural perspective. Both the Johnson[2j−m,10] and Mann[11] approaches agree that the lowest energy solution fluxional process results in the migration of the pair of CO bridges from one Fe−Fe edge to another. A superimposition view of two molecules of **3** with the bridging CO ligands on different Fe−Fe edges is shown in Figure 11. It can immediately be seen that, apart from two pairs of equatorial CO ligands, none of the remaining CO positions are very close. The closest C−C contacts (~1.5−1.7 Å) are marked by the broken lines in Figure 11. This path of closest contacts has some similarities with the S_{10} mechanism of Mann.[11] While it cannot be stated with certainty that the fluxional intermediate in the lowest energy process in **3** lies on the path of least motion indicated in Figure 11, it is intuitively reasonable to assume so. Given this assumption, it is also reasonable to suppose that the geometry of the intermediate/transition state will be approxi-

(43) The unit cell for this subset was the same as for the RT phase (a = 8.208(1) Å, b = 11.136(1) Å, c = 8.763(1) Å, β = 96.96(1)°, space group $P2_1/n$). The Cotton and Troup[2b] RT model was used, except that some extra disorder was observed and attributed to the Fe atoms of a second orientation of the molecule, present as ~7% of the population. Inclusion of this extra disordered component resulted in a lowering of the conventional R_F (observed) value from 0.057 to 0.028 and of the maximum electron density residual from 2.1 to 0.3 e Å^{-3}. This result led us to reexamine the 100 K high-resolution (θ_{max}= 40°) data set which we had previously[2c] collected using the incorrect (RT phase) unit cell. Similar residuals were found to be present; indeed, they were more obvious (peak heights 3.04−2.15 e Å^{-3}), although their significance was not appreciated at the time of our original report.[2c] The conventional R_F(observed) was reduced from 0.073 to 0.045, and the maximum residual electron density was reduced from 3.0 to ca. 0.8 e Å^{-3}. The population ratio of the primary to secondary images was refined to ~93:7. Thus, there is little doubt that the results from both data sets are very similar. Finally, to investigate whether any metal atom disorder might have previously been missed at room temperature, we obtained a data set for $Fe_3(CO)_{12}$ at 298 K. Refinement against these data, using the Cotton and Troup[2b] model, showed the highest residual in exactly the same position as that observed at low temperature. This peak height was somewhat smaller (ca. 1 e Å^{-3}) than at lower temperature, and the other two putative Fe atoms were only ~0.5 e Å^{-3}. It thus seems possible that the same disorder shown at low temperatures is also present at room temperature, albeit to a lesser extent.

mately halfway along this path. This "intermediate" is shown in Figure 12. There are two Fe−Fe edges with incipient CO bridges, with Fe···C contacts of ∼2.6 Å. It is a moot point as to whether the geometry of this "intermediate" is described as D_3, since the term is often used loosely in a qualitative and descriptive sense. Nevertheless, it is clearly very similar to complex **2** and even more similar to complex **8**.

In conclusion, the solid-state results reported in this paper provide some supporting evidence for both the Johnson[13] and Mann[11] proposals for the fluxionality of $Fe_3(CO)_{12}$. Perhaps this is not surprising, since these approaches may be alternative descriptions of the same process. The literature arguments[11,13] concerning these two mechanisms come down to subtle differences in the geometry of proposed transition states/intermediates which are very difficult to distinguish experimentally.

Acknowledgment. L.J.F. thanks the EPSRC (U.K.) for a grant toward the purchase of a diffractometer, and D.B. and F.G. thank MURST (Italy) for financial support. We also thank Professor A. G. Orpen (Bristol, U.K.) and Dr. S. J. Teat (Daresbury, U.K.) for assistance with collecting low-temperature diffraction data on $Fe_3(CO)_{12}$ using area detectors and Professor W. Clegg for making time available at the SRS, Daresbury, U.K.

Supporting Information Available: Tables of atomic coordinates and equivalent isotropic thermal parameters, anisotropic thermal parameters, and all bond lengths and bond angles for complexes **1**−**3** and Table S1, containing details of the TLS analyses. This material is available free of charge via the Internet at http://pubs.acs.org. Tables of observed and calculated structure factors are available from L.J.F. on request.

OM9902986